# Coherent Spin Preparation of Indium Donor Qubits in Single ZnO Nanowires

Maria L. K. Viitaniemi,[1,*] Christian Zimmermann,[1] Vasileios Niaouris,[1] Samuel H. D'Ambrosia,[1] Xingyi Wang,[2] E. Senthil Kumar,[3] Faezeh Mohammadbeigi,[3] Simon P. Watkins,[3] and Kai-Mei C. Fu[1,2]

[1] *Department of Physics, University of Washington, Seattle, Washington 98195, USA*
[2] *Department of Electrical Engineering, University of Washington, Seattle, Washington 98195, USA*
[3] *Department of Physics, Simon Fraser University, Burnaby, British Columbia V5A 1S6, Canada*

(Dated: January 10, 2022)

Shallow donors in ZnO are promising candidates for photon-mediated quantum technologies. Utilizing the indium donor, we show that favorable donor-bound exciton optical and electron spin properties are retained in isolated ZnO nanowires. The inhomogeneous optical linewidth of single nanowires (60 GHz) is within a factor of 2 of bulk single-crystalline ZnO. Spin initialization via optical pumping is demonstrated and coherent population trapping is observed. The two-photon absorption width approaches the theoretical limit expected due to the hyperfine interaction between the indium nuclear spin and the donor-bound electron.

arXiv:2110.13879v1 [quant-ph] 26 Oct 2021

Shallow donor spin qubits, composed of an electron bound to a donor ion, are one of the simplest solid-state qubit systems and have the potential for ultra-long qubit coherence times. For example, donors in silicon have demonstrated qubit coherence times from seconds [1] to minutes [2]. Unlike silicon, shallow neutral donors ($D^0$) in direct bandgap semiconductors exhibit efficient optical coupling to donor-bound excitons ($D^0X$). This coupling allows for the transfer of quantum information between the electron spin state and a photon, hence enabling photon-based applications in quantum communication [3] and computation [4]. The direct bandgap semiconductor ZnO is a particularly attractive host due to its large exciton binding energy [5], low spin-orbit coupling [6] and potential for a nuclear spin-free host with Zn isotope purification. Al, Ga, and In substituting for Zn are common shallow donors in ZnO, with In having the largest binding energy of the three [5].

Most quantum applications utilizing such optically-active donors will require the isolation of single donors [4, 7] and nanoscale device integration [8, 9]. However, obtaining good spin and optical properties for donors in nanostructures may be challenging; the extended effective-mass wave function of the donor and the resulting shallow donor binding energy leave the donor sensitive to surface noise [10, 11]. Here, we show the promise of utilizing a bottom-up technique to isolate a small ensemble of In donors. We demonstrate that the inhomogeneous In $D^0X$ linewidth in ensembles of nanowires (20 GHz) is comparable to the bulk single-crystalline $D^0X$ linewidth (15-25 GHz). Dropcasting to isolate single nanowires only increases the linewidth to 60 GHz. These narrow optical linewidths enable the optical probing of the spin properties of the donor ground-state. In single nanowires, we demonstrate spin initialization into both ground spin states via optical pumping [12, 13] and preparation of a coherent superposition spin state via coherent population trapping [14–17]. The measured 1 GHz two-photon absorption width approaches the limit expected due to the hyperfine interaction of the ground-state electron with the In spin-9/2 nuclear spin [18, 19].

* mariav93@uw.edu

ZnO nanowire samples are grown on a *c*-plane sapphire (0001) substrate via metal organic chemical vapor deposition (MOCVD) as described in [20]. Nanowires are typically 100-200 nm in diameter, 1-4 µm long, and grow in a dense ensemble. The ZnO crystal *c*-axis [0001] points along the long axis of the nanowire. A scanning electron micrograph (SEM) image of the nanowire ensemble is shown in inset (i) of Fig. 1c and in the supplementary material [21]. To isolate single nanowires, the ensemble sample is sonicated in ethanol to detach the nanowires from the sapphire substrate. The nanowires are then dropcast from the solution onto a $SiO_2$ substrate. An SEM image of a single dropcast nanowire is shown in inset (ii) of Fig. 1c. Isolation of single nanowires is achieved via scanning optical microscopy with representative laser reflection and photoluminescence images shown in Fig. 1b.

The nanowires are n-type due to unintentional doping during growth. In and Ga $D^0X$ lines are both present in the photoluminescence spectra (Fig. 1c); here, we focus on In due to its larger donor binding energy and higher concentration. The In donor concentration is estimated to have an upper limit of $10^{16}$ $cm^{-3}$ from nanoprobe resistivity measurements on similar samples.

Samples are mounted in a helium immersion cryostat with a superconducting magnet. Measurements are performed at 5.2 K. The magnetic field is aligned to the optical axis $\hat{k}$ ($\hat{k} \parallel \vec{B}$). Ensemble measurements are performed with the optical axis parallel to the crystal axis ($\hat{k} \parallel \hat{c}$). Because the single dropcast nanowires lie horizontally on the substrate, single nanowire measurements are performed with the optical axis (and magnetic field axis) perpendicular to the crystal axis ($\hat{c} \perp \hat{k}, \vec{B}$). We utilize a confocal microscope with a lateral point spread function of ∼1 µm. In the ensemble sample, this corresponds to approximately five nanowires on a floor of partially nucleated nanostructures (Fig. 1c inset (i)). In the single nanowire samples, we estimate that ensembles of a couple hundred indium donors are simultaneously addressed.

The energy level diagram of the In donor system is shown in Fig. 1a. The magnetic field lifts the spin degeneracy of the $D^0$ and the $D^0X$ states due to the electron and hole Zeeman effects [21–23], respectively. This leads to four $D^0$-

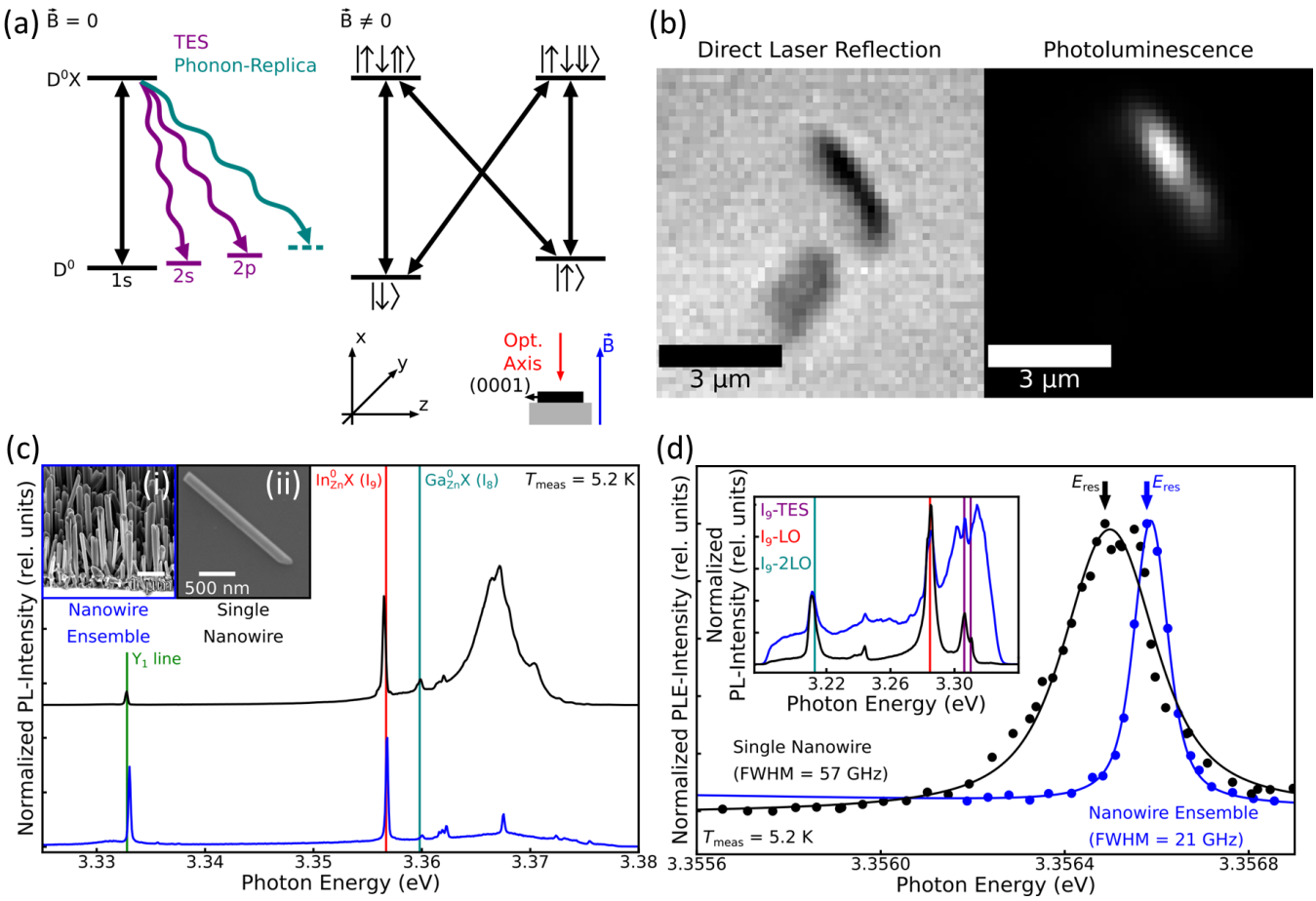



FIG. 1: (a) Energy level diagram of the $D^0$ and $D^0X$ system. The $|\uparrow\rangle$ ($|\Uparrow\rangle$) denotes the electron (hole) spin state. The diagram shows the experimental geometry for a single nanowire. (b) Confocal images of a single nanowire. Left panel: laser reflection is collected. Right panel: In $D^0X$ TES and LO-phonon replicas are collected under resonant excitation of the In $D^0X$ transition. (c) Spectra of an ensemble (blue) and single (black) nanowire with above-band gap excitation at 3.4440 eV, 5.2 K, and 0 T. The excitation power is 10 nW (36 nW) for the ensemble (single) nanowires. The single nanowire spectra has been offset for clarity. Labeled transitions are from [5]. The inset shows SEM images of an (i) ensemble and a (ii) single nanowire. (d) In $D^0X$ PLE spectra of an ensemble (blue) and single (black) nanowire at 5.2 K and 0 T. The solid lines are Voigt fits to the data. The inset shows the TES and LO-phonon replica spectrum with the excitation laser resonant on the In $D^0X$ transition. For the nanowire ensemble PLE, the broad non-specific background is subtracted from the spectrum before summing.

$D^0X$ transitions with nominally two polarized in each $\hat{y}$ and $\hat{z}$; however, these polarization rules are relaxed when coupling into the end of a nanowire. Moreover, the system may relax via several lower energy transitions such as the longitudinal-optical (LO) phonon replicas and the two electron satellite (TES) transitions (corresponding to relaxation to an excited hydrogenic $D^0$ orbital) [5].

Photoluminescence spectra of both the ensemble and single nanowire samples are shown in Fig. 1c. The In $D^0X$ transition is observed at 3.3567 eV. In addition to the In, Ga and Y-line donor-bound exciton features [5], the broad surface exciton is observed between 3.365-3.370 eV [24–27]. The inset in Fig. 1d shows the In $D^0X$ TES and LO-phonon replicas under resonant In $D^0X$ excitation. A striking contrast can be observed between the two samples. In the ensemble sample, the TES and LO-phonon replicas are on a large background which is uncorrelated with the In $D^0X$ transition. This background may be related to the thin 2-dimensional layer of ZnO on the ensemble substrate as well as to the observed non-uniformity of individual nanowires. For single nanowire measurements, nanowires are screened for sharp In $D^0X$ transitions and low non-specific background in the TES/LO-phonon replica region [21].

The In $D^0X$ linewidth can be spectrometer-resolution limited. To obtain higher-resolution spectra, we perform photoluminescence excitation spectroscopy (PLE). In PLE measurements, $D^0X$ TES and LO-phonon replicas are monitored while tuning the excitation laser wavelength over the In $D^0X$ transitions. For the nanowire ensembles, the non-specific background is subtracted and only the LO-phonon replicas are monitored. The excitation power is 200 nW (7.2 μW) for the ensemble (single) nanowires. We are able to use a

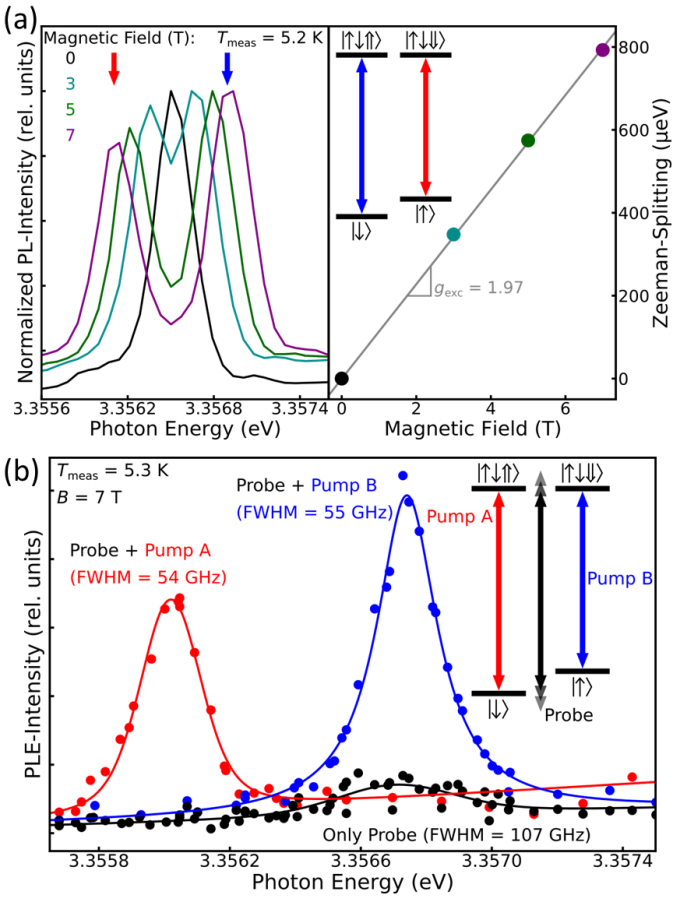



FIG. 2: (a) Magnetic field-dependent photoluminescence spectra of the In $D^0X$ transitions for a single nanowire at 5.2 K. Data are shown at 0 (black), 3 (teal), 5 (green), and 7 T (purple). The right panel shows the Zeeman splitting as a function of magnetic field. The gray line is a fit to the data which yields the sum of the electron and hole $g$-factors. (b) Single nanowire PLE spectra of the In $D^0X$ transitions at 7 T, 5.3 K with no pump (black), pump on the high energy transition (red), and pump on the low energy transition (blue) are shown. All laser powers are 7.2 μW. The two-laser datasets (red and blue) are offset for ease of comparison. The CPT dip is not visible because of the low spectral resolution.

lower excitation power for the ensemble nanowires, because of the larger volume of material within our measurement spot and the increased collection efficiency from the top of the nanowires due to wave-guiding (see supplementary material [21]). As shown in Fig. 1d, in nanowire ensembles, PLE linewidths of 20 GHz are measured. These are comparable to the narrowest linewidths (15-25 GHz) measured in our lab on bulk single-crystalline ZnO for Ga $D^0X$ transitions at 5 K [21]. In single nanowires, linewidths as narrow as 57 GHz are observed. We attribute the increase in linewidth to additional strain caused by the dropcasting process as well as spectral diffusion and several homogeneous broadening mechanisms we will discuss further below. Due to the high non-specific background in the ensemble TES/LO-phonon replica region as well as the ability to isolate fewer donors in the isolated nanowires, we focus on single nanowire measurements for the remainder of this work.

In order to utilize the $D^0$ system for quantum applications, the spin degeneracy of the $D^0$ and $D^0X$ states must be lifted. A magnetic field may be used to split the ground state as determined by the electron $g$-factor ($g_e$). The splitting of the excited state is then solely determined by the hole $g$-factor ($g_h$), because the excited state electrons form a spin singlet. As shown in Fig. 2a, when a magnetic field is applied perpendicular to the crystal $c$-axis, the sum of $g_e$ and $g_h^\perp$ is measured to be $g_{tot} = 1.97$ in a single nanowire. This is consistent with reported values for $g_e$ (1.9-2.0) and the lowest values reported for $g_h^\perp$ (0.1-0.3) [22, 23]. As described later in the text, we use high-resolution PLE to further confirm a $g_e$ of 1.90 and therefore a lower bound for $g_h^\perp$ of 0.07.

When a magnetic field is applied to the donor system, the spin degeneracy is lifted and donor spin initialization can be performed by resonant optical pumping [12, 13]. For example, to optically pump the system into the $|\downarrow\rangle$ state, a resonant laser may be applied to the $|\uparrow\rangle \Leftrightarrow |\Downarrow\uparrow\downarrow\rangle$ transition. Because the $D^0X$ state can relax into either $D^0$ spin state [23], after several cycles, the spin is initialized to the $|\downarrow\rangle$ state. Fig. 2b shows three PLE spectra which confirm that optical pumping can be achieved in a single nanowire. First, we perform a single-laser scan over the $D^0X$ transitions at 7 T (black data). Due to the small observed hole splitting, we expect the two transitions sharing the same electron spin ground-state level will not be resolved. For these single-laser, steady-state measurements, we also expect the PLE intensity to be significantly weaker at 7 T than it was at 0 T due to optical pumping. For the pair of transitions involving the $|\uparrow\rangle$ state, the signal lies below the noise floor. To confirm that the overall low signal is due to optical pumping, we perform two-laser spectroscopy. A resonant pump laser is applied on the $|\downarrow\rangle \Leftrightarrow |\Uparrow\uparrow\downarrow\rangle$ transition while a second probe laser is scanned over all the In $D^0X$ transitions (red data). In this two-laser PLE, the pump laser is able to re-pump population from $|\downarrow\rangle$ to $|\uparrow\rangle$ so that the $|\uparrow\rangle \Leftrightarrow |\Downarrow\uparrow\downarrow\rangle$ transition signal is recovered. A similar phenomenon can be observed by placing the pump laser on the $|\uparrow\rangle \Leftrightarrow |\Downarrow\uparrow\downarrow\rangle$ transition and recovering the $|\downarrow\rangle \Leftrightarrow |\Uparrow\uparrow\downarrow\rangle$ transition signal (blue data). The 7 T two-laser linewidth of 55 GHz corresponds to the spectral diffusion and homogeneously broadened linewidth of the donor subpopulation that is optically pumped. This is within the uncertainty of the 57 GHz 0 T single nanowire PLE linewidth (Fig. 1d) which includes static inhomogeneous broadening from the entire donor ensemble. The similarity between the 0 T single-laser and the 7 T two-laser linewidths suggest broadening mechanisms, such as power broadening [28], laser-induced temperature broadening, and spectral diffusion that is fast compared to our measurement time (20 s) [29–31], are the dominant line broadening mechanisms in all of the single nanowire spectra. All of these mechanisms may be exacerbated by the higher powers used for single nanowire measurements relative to the ensemble nanowire measurements.

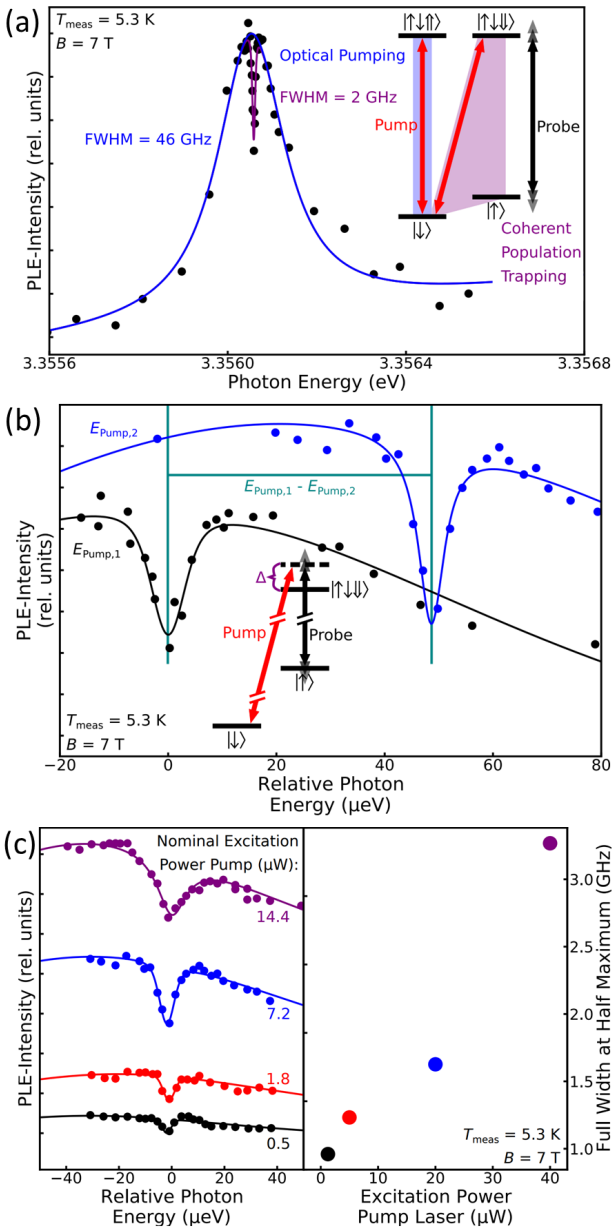



FIG. 3: Single nanowire, high resolution PLE spectra of the In $D^0X$ transitions at 7 T, 5.3 K. All laser powers are 7.2 μW unless otherwise noted. (a) PLE showing the CPT dip. The pump laser is on resonance with the $|\downarrow\rangle \Leftrightarrow |\Uparrow\uparrow\downarrow\rangle$ transition. (b) PLE over the CPT dip with the pump laser wavelength at 3.35687 eV (3.35682 eV) for the black $E_{Pump,1}$ (blue $E_{Pump,2}$) data. (c) The left panel shows PLE spectra over the CPT dip with the pump laser wavelength at 3.35774 eV. The power of the pump laser is 14.4, 7.2, 1.8, and 0.5 μW (from top to bottom).

High-resolution two-laser scans, shown in Fig. 3a, reveal a sharp 2 GHz wide dip on the PLE peak that is the result of coherent population trapping (CPT). In CPT, the system enters a dark state when the two transitions of a Λ system are simultaneously pumped [14–17]. For example, the Λ system can be formed between the two electron ground states and a single excited $D^0X$ state. In our experiments, because the Zeeman splitting between the $D^0X$ states is small relative to the two-laser linewidth (Fig. 2b), the pump laser is able to excite both $|\downarrow\rangle \Leftrightarrow |\Uparrow\uparrow\downarrow\rangle$ and $|\downarrow\rangle \Leftrightarrow |\Downarrow\uparrow\downarrow\rangle$ simultaneously; therefore, as shown in the inset to Fig. 3a, a Λ system is formed by the pump laser driving $|\downarrow\rangle \Leftrightarrow |\Downarrow\uparrow\downarrow\rangle$ and the probe laser on $|\uparrow\rangle \Leftrightarrow |\Downarrow\uparrow\downarrow\rangle$.

To confirm that the dip is related to CPT, we detune the pump laser energy by Δ from $|\downarrow\rangle \Leftrightarrow |\Downarrow\uparrow\downarrow\rangle$ and measure the shift of the dip (Fig. 3b). We observe a one-to-one correlation between Δ and the spectral position of the dip [21]. As expected, the separation between the pump energies and the dip energies (0.76-0.77 meV) is consistent with a $g_e$ of 1.90 [23], confirming a lower bound for $g_h^{\perp}$ of 0.07. Moreover, Fig. 3c shows that reducing the pump laser power reduces the dip linewidth and contrast as expected in CPT [14, 32]. The smallest linewidth (1 GHz) approaches the linewidth expected due to the spin-9/2 In nuclear-electron hyperfine interaction, where the In line splits into 10 hyperfine lines separated by 100 MHz each [18, 19]. Moreover, considering spectral diffusion as a broadening mechanism for the two-laser peak (Fig. 2b), the narrowness of the CPT dip (1 GHz) compared to the two-laser peak (55 GHz) rules out ground-state spectral diffusion; therefore, excited-state spectral diffusion is the dominant spectral diffusion mechanism.

In summary, In donors in single ZnO nanowires preserve several important properties for utilizing donor spins in direct band gap materials as qubits. Photoluminescence excitation linewidths comparable to bulk show that even in the proximity of surfaces, high optical homogeneity is retained. Optical spin initialization and coherent population trapping are essential steps towards the spin control needed to prepare arbitrary qubit states. We expect higher collection efficiencies and cleaner selection rules can be achieved by moving towards single nanowires in a vertical geometry [21]. This would allow us to use lower excitation powers, minimizing the observed linewidth broadening and surface exciton. Additionally, there are several avenues to continue toward the single donor limit, including increasing the purity of the ZnO precursor materials or the study of two lattice-site donor defects, like the tin complex [33], that have lower probabilities of formation.

## I. SUPPORTING INFORMATION

SEMs of ensemble nanowires, photoluminescence spectra of additional nanowires, description of background correction, 0 T photoluminescence spectra of the TES/LO-phonon replica region with resonant excitation, comparison of 0 T PLE on various samples, magnetic field dependent spectra to measure the g-factor in ensemble nanowires, photoluminescence spectra of the TES/LO-phonon replica region at 7 T with 2-laser resonant excitation, optical pumping demonstration of the nanowire ensemble and an additional nanowire, low-resolution 2-laser PLE measurements with varying pump wavelength, CPT measurements on an additional nanowire, CPT measurements on the main text nanowire with additional pump wavelengths, and simulation

of light-guiding in a nanowire.

## II. ACKNOWLEDGEMENTS

We would like to thank Yusuke Kozuka for the bulk ZnO samples used for comparison, Ethan Hansen for assistance in performing PLE and PL measurements on ZnO nanowire ensembles, and Xiayu Linpeng for fruitful discussions. The support of the Natural Sciences and Engineering Research Council of Canada is gratefully acknowledged. This material is based upon work primarily supported by the Army Research Office MURI Grant on Ab Initio Solid-State Quantum Materials: Design, Production and Characterization at the Atomic Scale (18057522). Bulk measurements were supported by National Science Foundation under Grant No. 1150647.

[1] Alexei M. Tyryshkin, Shinichi Tojo, John J.L. Morton, Helge Riemann, Nikolai V. Abrosimov, Peter Becker, Hans Joachim Pohl, Thomas Schenkel, Michael L.W. Thewalt, Kohei M. Itoh, and S. A. Lyon, "Electron spin coherence exceeding seconds in high-purity silicon," Nature Materials **11**, 143–147 (2012).

[2] Kamyar Saeedi, Stephanie Simmons, Jeff Z Salvail, Phillip Dluhy, Helge Riemann, Nikolai V Abrosimov, Peter Becker, Hans-Joachim Pohl, John J L Morton, and Mike L W Thewalt, "Room-temperature quantum bit storage exceeding 39 minutes using ionized donors in silicon-28," Science **342**, 830–833 (2013).

[3] Stephanie Wehner, David Elkouss, and Ronald Hanson, "Quantum internet: A vision for the road ahead," Science **362** (2018), 10.1126/science.aam9288.

[4] Simon C. Benjamin, Brendon W. Lovett, and Jason M. Smith, "Prospects for measurement-based quantum computing with solid state spins," Laser & Photonics Reviews **3**, 556–574 (2009).

[5] Bruno K. Meyer, H. Alves, D. M. Hofmann, W. Kriegseis, D. Forster, F. Bertram, J. Christen, A. Hoffmann, M. Straßburg, M. Dworzak, U. Haboeck, and A. V. Rodina, "Bound exciton and donor-acceptor pair recombinations in ZnO," Physica Status Solidi (B) **241**, 231–260 (2004).

[6] Alexander V. Khaetskii and Yuli V. Nazarov, "Spin-flip transitions between Zeeman sublevels in semiconductor quantum dots," Phys. Rev. B **64**, 125316 (2001).

[7] T. D. Ladd, F. Jelezko, R. Laflamme, Y. Nakamura, C. Monroe, and J. L. O'Brien, "Quantum computers," Nature **464**, 45–53 (2010).

[8] Emma R. Schmidgall, Srivatsa Chakravarthi, Michael Gould, Ian R. Christen, Karine Hestroffer, Fariba Hatami, and Kai Mei C. Fu, "Frequency control of single quantum emitters in integrated photonic circuits," Nano Letters **18**, 1175–1179 (2018).

[9] Tim Schröder, Sara L. Mouradian, Jiabao Zheng, Matthew E. Trusheim, Michael Walsh, Edward H. Chen, Luozhou Li, Igal Bayn, and Dirk Englund, "Quantum nanophotonics in diamond [invited]," Journal of the Optical Society of America B **33**, B65–B83 (2016).

[10] B E Kane, "A silicon-based nuclear spin quantum computer," Nature **393**, 133–137 (1998).

[11] A K Ramdas and S Rodriguez, "Spectroscopy of the solid-state analogues of the hydrogen atom: donors and acceptors in semiconductors," Reports on Progress in Physics **44**, 1297–1387 (1981).

[12] Xiayu Linpeng, Todd Karin, M V Durnev, Russell Barbour, M M Glazov, E Ya Sherman, S P Watkins, Satoru Seto, and Kai-Mei C Fu, "Longitudinal spin relaxation of donor-bound electrons in direct band-gap semiconductors," Physical Review B **94**, 125401–125420 (2016).

[13] Darin J. Sleiter, Kaoru Sanaka, Y. M. Kim, Klaus Lischka, Alexander Pawlis, and Yoshihisa Yamamoto, "Optical pumping of a single electron spin bound to a fluorine donor in a ZnSe nanostructure," Nano Letters **13**, 116–120 (2013).

[14] Kai Mei C Fu, Charles Santori, Colin Stanley, M C Holland, and Yoshihisa Yamamoto, "Coherent population trapping of electron spins in a high-purity n-type GaAs semiconductor," Physical Review Letters **95**, 187405–187409 (2005).

[15] Charles Santori, Philippe Tamarat, Philipp Neumann, Jörg Wrachtrup, David Fattal, Raymond G. Beausoleil, James Rabeau, Paolo Olivero, Andrew D. Greentree, Steven Prawer, Fedor Jelezko, and Philip Hemmer, "Coherent population trapping of single spins in diamond under optical excitation," Physical Review Letters **97**, 247401–247405 (2006).

[16] H R Gray, R M Whitley, and C R Stroud, "Coherent trapping of atomic populations," Optics Letters **3**, 218–220 (1978).

[17] Xiaodong Xu, Bo Sun, Paul R. Berman, Duncan G. Steel, Allan S. Bracker, Dan Gammon, and L. J. Sham, "Coherent population trapping of an electron spin in a single negatively charged quantum dot," Nature Physics **4**, 692–695 (2008).

[18] C. Gonzalez, D. Block, R. T. Cox, and A. Hervé, "Magnetic resonance studies of shallow donors in zinc oxide," Journal of Crystal Growth **59**, 357–362 (1982).

[19] D Block, A Hervé, and R T Cox, "Optically detected magnetic resonance and optically detected endor of shallow indium donors in ZnO," Physical Review B **25**, 6049–6052 (1982).

[20] E Senthil Kumar, F Mohammadbeigi, S Alagha, Z W Deng, I P Anderson, T Wintschel, and S P Watkins, "Optical evidence for donor behavior of Sb in ZnO nanowires," Applied Physics Letters **102**, 132105 (2013).

[21] See Supplementary Material.

[22] L. Ding, B. K. Li, H. T. He, W. K. Ge, J. N. Wang, J. Q. Ning, X. M. Dai, C. C. Ling, and S. J. Xu, "Classification of bound exciton complexes in bulk ZnO by magnetophotoluminescence spectroscopy," Journal of Applied Physics **105**, 053511 (2009).

[23] Markus R. Wagner, Jan Hindrik Schulze, Ronny Kirste, Munise Cobet, Axel Hoffmann, Christian Rauch, Anna V. Rodina, Bruno K. Meyer, Uwe Röder, and Klaus Thonke, "$\Gamma_7$ valence band symmetry related hole fine splitting of bound excitons in ZnO observed in magneto-optical studies," Physical Review B **80**, 205203–205209 (2009).

[24] L. Wischmeier, T. Voss, I. Rückmann, J. Gutowski, A. C. Mofor, A. Bakin, and A. Waag, "Dynamics of surface-excitonic emission in ZnO nanowires," Physical Review B **74**, 195333–195342 (2006).

[25] Mahua Biswas, Yun Suk Jung, Hong Koo Kim, Kumarappan Kumar, Gregory J. Hughes, S. Newcomb, Martin O. Henry,

and Enda McGlynn, "Microscopic origins of the surface exciton photoluminescence peak in ZnO nanostructures," Physical Review B **83**, 235320–235330 (2011).

[26] J. Grabowska, A. Meaney, K. K. Nanda, J. P. Mosnier, M. O. Henry, J. R. Duclère, and E. McGlynn, "Surface excitonic emission and quenching effects in ZnO nanowire/nanowall systems: Limiting effects on device potential," Physical Review B **71**, 115439–115446 (2005).

[27] V.V. Travnikov, A. Freiberg, and S.F. Savikhin, "Surface excitons in ZnO crystals," Journal of Physics: Condensed Matter **1**, 847–854 (1989).

[28] M. E. Reimer, G. Bulgarini, A. Fognini, R. W. Heeres, B. J. Witek, M. A.M. Versteegh, A. Rubino, T. Braun, M. Kamp, S. Höfling, D. Dalacu, J. Lapointe, P. J. Poole, and V. Zwiller, "Overcoming power broadening of the quantum dot emission in a pure wurtzite nanowire," Physical Review B **93**, 195316 (2016).

[29] M. Holmes, S. Kako, K. Choi, M. Arita, and Y. Arakawa, "Spectral diffusion and its influence on the emission linewidths of site-controlled GaN nanowire quantum dots," Physical Review B **92**, 115447–115454 (2015).

[30] S. A. Empedocles and M. G. Bawendi, "Influence of spectral diffusion on the line shapes of single CdSe nanocrystallite quantum dots," Journal of Physical Chemistry B **103**, 1826–1830 (1999).

[31] Evan MacQuarrie, Camille Chartrand, Daniel Higginbottom, Kevin Morse, Valentin Karasyuk, Sjoerd Roorda, and Stephanie Simmons, "Generating T centres in photonic silicon-on-insulator material by ion implantation," New Journal of Physics **23**, 103008 (2021).

[32] Xiayu Linpeng, Todd Karin, Mikhail V. Durnev, Mikhail M. Glazov, Rüdiger Schott, Andreas D. Wieck, Arne Ludwig, and Kai Mei C. Fu, "Optical spin control and coherence properties of acceptor bound holes in strained GaAs," Physical Review B **103**, 115412–115422 (2021).

[33] E. Senthil Kumar, F. Mohammadbeigi, L. A. Boatner, and S. P. Watkins, "High-resolution photoluminescence spectroscopy of Sn-doped ZnO single crystals," Journal of Luminescence **176**, 47–51 (2016).

arXiv:2110.13879v1 [quant-ph] 26 Oct 2021

# Supplementary Information

Maria L. K. Viitaniemi,[1,*] Christian Zimmermann,[1] Vasileios Niaouris,[1] Samuel H. D'Ambrosia,[1] Xingyi Wang,[2] E. Senthil Kumar,[3] Faezeh Mohammadbeigi,[3] Simon P. Watkins,[3] and Kai-Mei C. Fu[1,2]

[1] *Department of Physics, University of Washington, Seattle, Washington 98195, USA*
[2] *Department of Electrical Engineering, University of Washington, Seattle, Washington 98195, USA*
[3] *Department of Physics, Simon Fraser University, Burnaby, British Columbia V5A 1S6, Canada*

(Dated: January 10, 2022)

## I. NANOWIRE ENSEMBLE SAMPLE

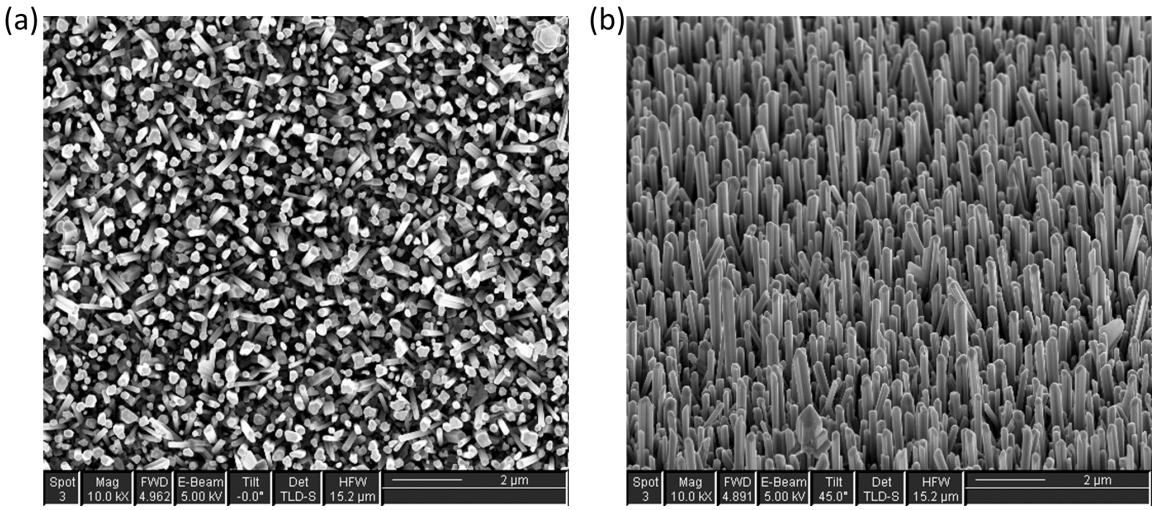



FIG. 1: Scanning electron micrograph images of the ensemble nanowire sample (a) from directly above and (b) from a 45 degree angle.

* mariav93@uw.edu

## II. NANOWIRE SURVEY USING PHOTOLUMINESCENCE SPECTRA UNDER ABOVE-BAND GAP EXCITATION

Fig. 2 displays normalized photoluminescence spectra recorded on single dropcast nanowires and a nanowire ensemble. The excitation laser energy was 3.4440 eV which is larger than the band gap of ZnO. Different single nanowires differ in the relative intensities of the surface exciton, Y-line, and In $D^0$-$D^0X$ peak. Moreover, a broadening and splitting of the In $D^0$-$D^0X$ and Y-line transitions can be observed for some single nanowires. This broadening and splitting is not observed in nanowire ensembles. Thus, we propose that the broadening and splitting of the In $D^0$-$D^0X$ and Y-line transitions in the single nanowires is related to strain caused by the dropcasting process. In the main article, we mainly discuss results from nanowire 18, because it displays a In $D^0$-$D^0X$ transition lineshape comparable to the nanowire ensemble sample.

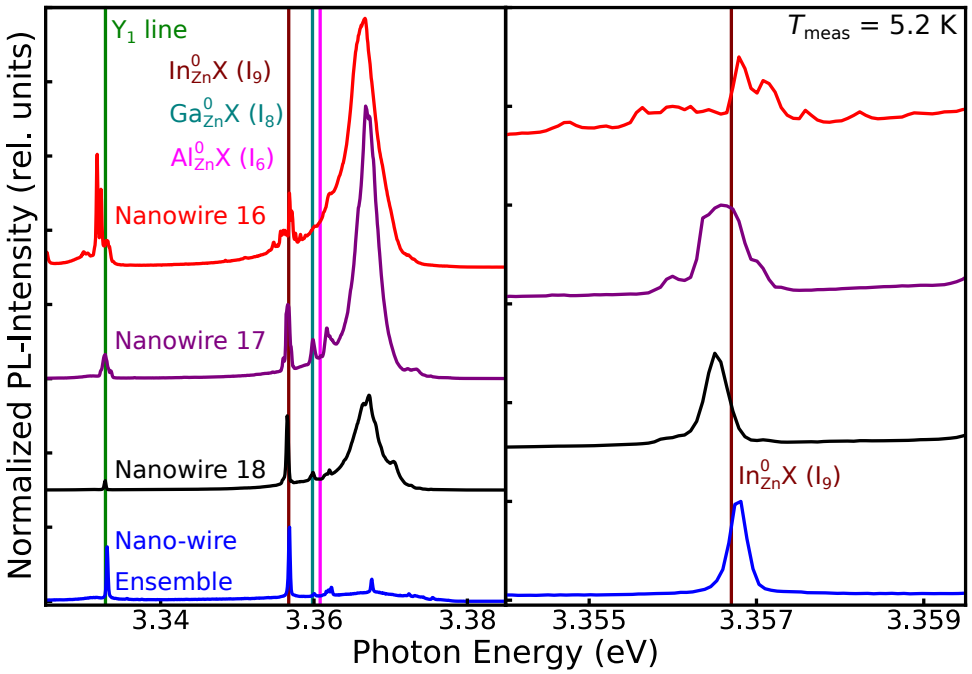



FIG. 2: Photoluminescence spectra of several different dropcast nanowires (red, purple, and black) and the nanowire ensemble (blue). All measurements are normalized to the height of the In $D^0$-$D^0X$ peak. All measurements are performed at 0 T and 5.2 K with an excitation laser energy of 3.4440 eV. The excitation power was 36 nW for the single nanowires and 10 nW for the nanowire ensemble. The right panel is zoomed in to better observe the differences in the In $D^0$-$D^0X$ peak. The line identifications are from [1].

## III. OSCILLATORY BACKGROUND CORRECTION

A wavelength-dependent modulation of the signal is observed in single nanowire photoluminescence excitation (PLE) data. This is a consequence of a wavelength dependence of the transmittance and reflectance of the beamsplitter used in the excitation path. During the single nanowire measurements, the laser power was held constant at $P_C$ (Fig. 3b), leading to an oscillation in the excitation power, $P_A$. In order to correct for this oscillation in the excitation power, the wavelength dependence of the ratio of the reflected to transmitted power for the beamsplitter was measured. Fig. 3a shows a representative measurement. The wavelength dependence of $P_A/P_B$ was found to have minimal variation in offset, amplitude, and period, while the phase was found to change significantly between measurements, possibly depending on factors such as ambient temperature.

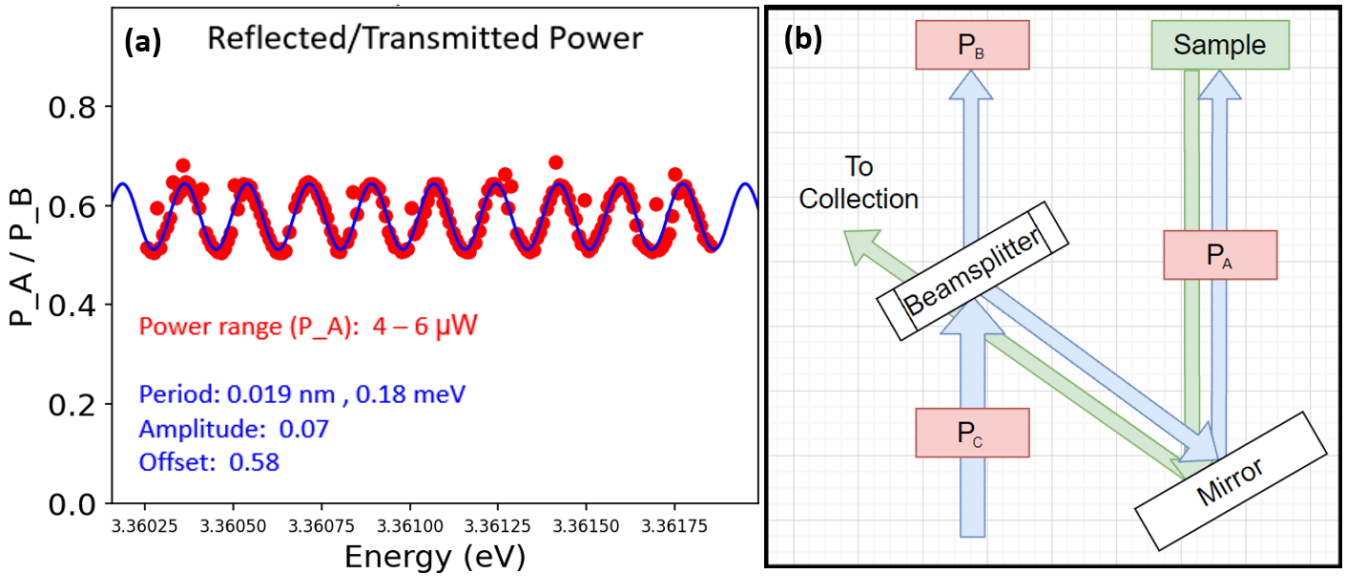



FIG. 3: (a) A measurement of wavelength dependence of excitation path beamsplitter transmitted and reflected powers. (b) Schematic of excitation path with power meter positions.

Correction of this oscillation was only applied to single-nanowire data where power was measured at $P_C$ rather than $P_A$. Assuming minimal absorption and scattering from the beamsplitter, and only phase changes in $P_A/P_B$, oscillations in the excitation power can be calculated. For simplicity, we will use $f(\mathrm{E}, \phi)$ for handling $P_A/P_B$, using the data in Fig. 3 to define the function. $E$ is the excitation photon energy, and $\phi$ is the phase of the oscillation.

$$f(E,\phi) = \frac{\mathrm{P_A}}{\mathrm{P_B}} = 0.58 + 0.07 \times \sin\left(\frac{2\pi E}{0.18\mathrm{meV}} + \phi\right)$$

Minimal absorption and scattering tells us $\mathrm{P_C} = \mathrm{P_A} + \mathrm{P_B}$, thus $\mathrm{P_C} = \mathrm{P_A}\ (1 + 1/f(\mathrm{E}, \phi))$. The mean power reflected over incident power $\mathrm{P_A/P_C}$ is 0.36. This factor can be used to convert from an oscillating excitation power to a constant excitation power, as $\mathrm{P_C}$ was held constant during measurement. The oscillatory background correction is performed by determining the phase of $f(\mathrm{E}, \phi)$, then multiplying the measured PLE intensity by the resulting energy dependent correction factor.

$$\frac{\text{Corrected } \mathrm{P_A}}{\mathrm{P_A}} = (1 + \frac{1}{f(E,\phi)}) \cdot (0.36) = \text{Correction Factor}$$

In the regime where the PLE intensity is proportional to the probe power, PLE data can be accurately corrected using this factor. The probe power changes by 18% peak to peak. This small variation in excitation power from the oscillation allows for the approximation of the dependence of the PLE intensity on probe power as linear, $\mathrm{Counts}(E) \approx \alpha P_A(E) + \beta$. For single-laser PLE and for two-laser PLE with observable oscillations in the off-resonant signal, we find that $\alpha >> \beta$ and have therefore corrected the oscillations. Two-laser PLE with no observable oscillations were assumed to have $\alpha << \beta$ and have not been corrected.

This correction is applied in Fig. 4. First the off-resonant or background region is differentiated from the on-resonant

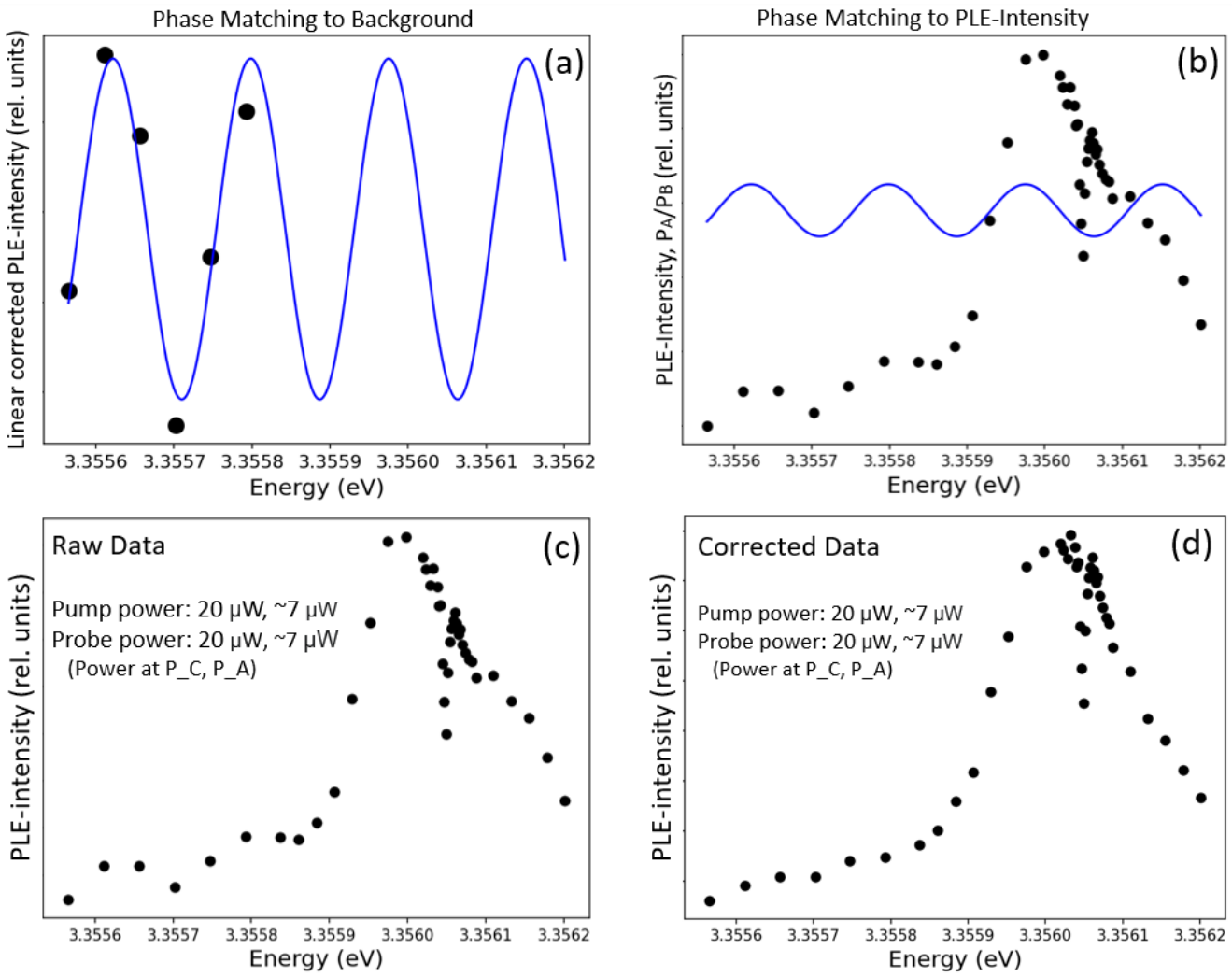



FIG. 4: (a) Sine fit with fixed period for determination of oscillation phase from linear corrected background PLE intensity. (b) Comparison of the phase and period of $P_A/P_B$ with low-energy background of the PLE intensity. Two oscillations in the background can be seen to the left of the peak, matching the phase and period of the correction, shown in blue. (c,d) Example data from the measurement of CPT on the In $D^0X$ in a single nanowire (c) before and (d) after correction.

or peak region. The background region is then linearly corrected and fit using a sine function with a period of 0.18 meV (Fig. 4a). From this fit the phase of $P_A/P_B$ is obtained, so our correction factor is determined. The resulting $P_A/P_B$ can be compared to PLE intensity to check that the oscillations align well with the low energy portion of the data, which was considered part of the background (Fig. 4b). Only the period and phase of $P_A/P_B$ is checked at this stage. Using the determined $P_A/P_B$, the PLE intensity is multiplied by the correction factor. The effect of this correction can be seen in Fig. 4c and Fig. 4d.

## IV. RESONANT EXCITATION

Fig. 5 displays photoluminescence spectra within the two electron satellite (TES) and longitudinal optical (LO) phonon replica spectral region for a single nanowire and a nanowire ensemble. Spectra were recorded with the excitation laser on- and off-resonance with the In $D^0$-$D^0X$ transition. For both, nanowire ensembles and single nanowires, the TES and phonon replica are enhanced in the on-resonance case compared to the off-resonance case. For the nanowire ensemble, a non-specific background can be seen in the on- and off-resonance cases. This non-specific background makes monitoring resonant excitation more challenging for nanowire ensembles. Some single nanowires also show a strong non-specific background similar to the nanowire ensemble. For this study, we screened the dropcast single nanowires for the presence of the non-specific background and only performed two-laser spectroscopy on single nanowires with a negligible non-specific background.

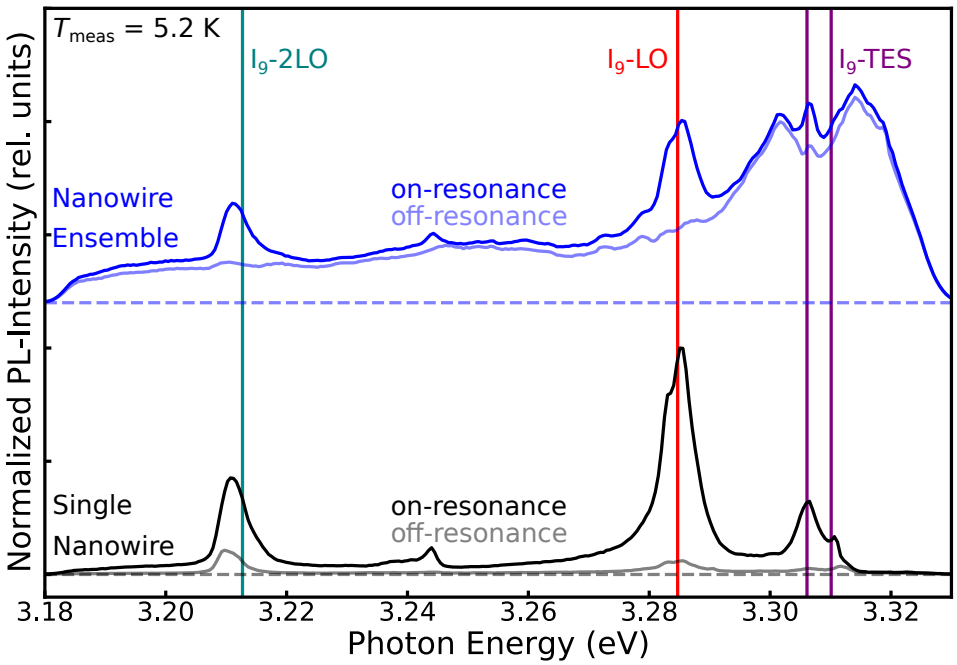



FIG. 5: Photoluminesence spectra of the two electron satellite (TES) and longitudinal-optical (LO) phonon replica spectral region for a single nanowire (bottom black) and the nanowire ensemble (top blue). The ensemble data has been offset for clarity. A dashed line indicates zero intensity for the corresponding data set. All measurements are at 0 T and 5.2 K. The excitation power is 7.2 µW (200 nW) for the single nanowire (ensemble) measurements. The darker (lighter) data is with the excitation laser on-(off-)resonance with the In $D^0$-$D^0X$ peak. A large non-specific background is visible for the nanowire ensemble region for both the on- and off-resonance spectra.

Fig. 6 displays photoluminescence excitation (PLE) spectra recorded on hydrothermally-grown single-crystalline bulk Tokyo Denpa ZnO, a single nanowire, and a nanowire ensemble. For the single crystals, PLE spectra were recorded for the Ga $D^0$-$D^0X$ transition; whereas for the single nanowire and nanowire ensemble, the measurements were performed for the In $D^0$-$D^0X$ transition. The spectral resolution of these scans is well below our laser linewidth of <1 MHz. The linewidths seen using single-laser PLE measurements at 0 T are a good indication of the inhomogeneous broadening. The linewidth observed for the nanowire ensemble is comparable to the linewidth seen for different ZnO bulk crystals, indicating that the inhomogeneous broadening observed for nanowire ensembles is comparable to that of some commercially-available, single-crystalline bulk ZnO. The single nanowire (nanowire #18 from Fig. 2) displays a significantly broadened linewidth, indicating additional inhomogeneous broadening mechanisms as compared to the nanowire ensemble. In accordance with the results presented in the main text, we propose strain introduced during the dropcasting process to be the source of this additional inhomogeneous broadening.

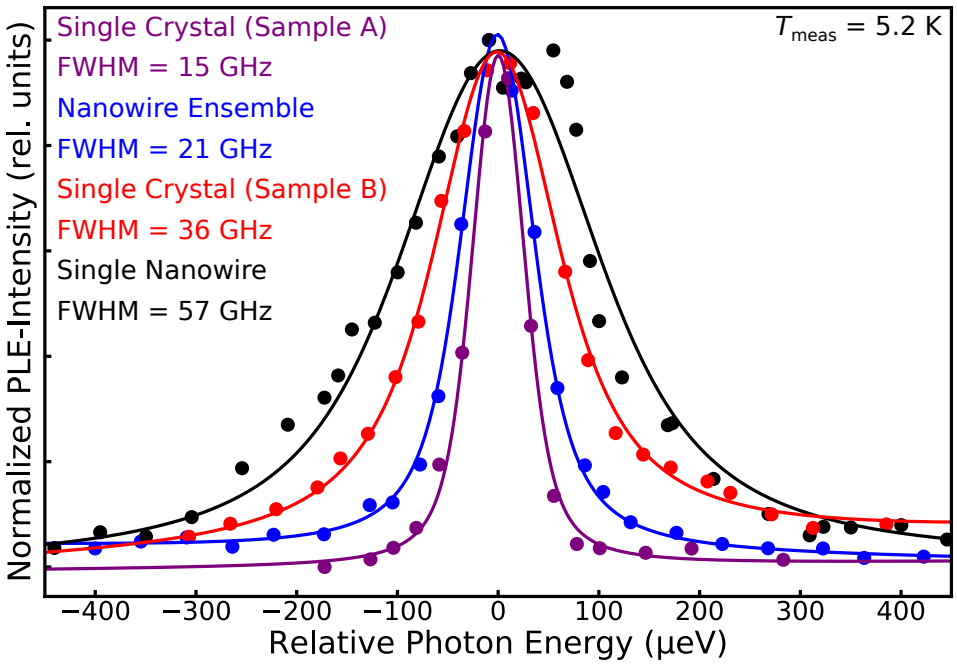



FIG. 6: Photoluminesence excitation (PLE) spectroscopy of bulk samples (purple and red), ensemble nanowire sample (blue), and single dropcast nanowire (nanowire #18 from Fig. 2) (black). All measurements are performed at 0 T and 5.2 K. For the bulk measurements, the excitation laser is scanned over the Ga $D^0$-$D^0X$ peak with 100 nW while the TES and LO-phonon replica luminescence is collected. For the single dropcast nanowire measurements, the excitation laser is scanned over the In $D^0$-$D^0X$ peak with 7.2 μW while the TES and LO-phonon replica luminescence is collected. For the nanowire ensemble measurements, the excitation laser is scanned over the In $D^0$-$D^0X$ peak with 200 nW. For the nanowire ensemble measurements only, the non-specific background is subtracted and only the two-LO-phonon replica luminescence is collected. The solid lines are fits to the data. The full width at half maximum (FWHM) for each data set is listed. The nanowire ensemble data and the single dropcast nanowire data are reproduced from the main text.

## V. POLARIZATION-DEPENDENT PHOTOLUMINESCENCE AT MAGNETIC FIELD

Photoluminescence measurements were performed on a nanowire ensemble at 7 T ($\hat{c} \perp \vec{B}$ and $\hat{c} \parallel \hat{k}$) using laser excitation at 3.4440 eV, i.e., using laser excitation above the band gap of ZnO. At 7 T, the spin degeneracies of the In $D^0$-$D^0X$ system are lifted and four transitions can be detected (see inset of Fig. 7a). For this measurement geometry, the transitions display linear polarizations, whereby two transitions are polarized horizontally and two transitions are polarized vertically. A half-wave plate in the collection and excitation path in combination with a linear polarizer in the collection path (set to V) were used to measure the polarization dependence of the photoluminescence spectra and the results are displayed in Fig. 7. We assume that the polarization of the excitation has no major effect, and that the main effect of the half-wave plate in combination with the linear polarizer is to select which transitions are collected (either H or V).

The left panel of Fig. 7a shows two distinct peaks; their separation is a result of the electron Zeeman splitting. The right panel of Fig. 7a shows a zoomed-in spectra of the high-energy peak. The black and teal arrows indicate the observed shift in peak maximum with polarization; this shift is a result of the hole Zeeman splitting. Fig. 7b shows the full polarization dependence of the peak maxima. Notably, the high-energy peak displays a more pronounced polarization dependence compared to the low-energy peak.

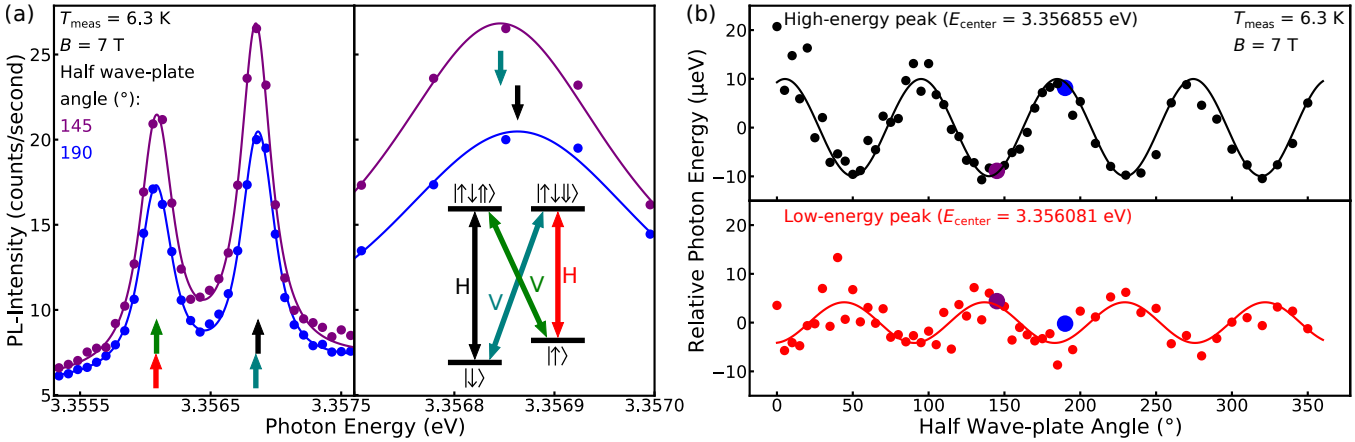



FIG. 7: Polarization-dependent photoluminescence measurements were performed on a nanowire ensemble at 7 T ($\hat{c} \perp \vec{B}$ and $\hat{c} \parallel \hat{k}$) and 6.3 K using laser excitation at 3.4440 eV and 40 nW. (a) Photoluminescence spectra are shown for two different positions of the half-wave plate. Left panel: Two distinct lines are observed originating from In $D^0X$ transitions involving the split ground-states. The lines are denoted as low-energy and high-energy peak. Right panel: A zoomed-in version of the left panel is shown to demonstrate the shift observed in the high-energy peak for different polarizations; this shift originates from the splitting of the excited state of the In $D^0$-$D^0X$ system. The arrows indicate the spectral maximums of the transitions shown with the same color. The inset illustrates the different transitions and their polarizations. H (V) stands for horizontally (vertically) polarized light. (b) The relative change in the position of the low- and high-energy peak seen in (a) as a function of the angle of the half-wave plate is displayed. The position of the low- and high-energy feature seen in (a) was determined using a voigt fit. The data points marked in purple and blue correspond to the spectra displayed in (a). Polarization selectivity is observed.

The data shown in Fig. 7b can be modelled with

$$E_{\mathrm{pos,i}} = E_{\mathrm{center,i}} + \Delta E_{\mathrm{excited,i}} \times \sin\left(a_{\mathrm{i}}\varphi + b_{\mathrm{i}}\right) \quad (\mathrm{i} = \mathrm{low},\ \mathrm{high}),$$

where $E_{\mathrm{pos,i}}$ is the position of the low-energy (i = low) or high-energy peak (i = high). $\varphi$ is the angle of the half-wave plate. $a_{\mathrm{i}}$ and $b_{\mathrm{i}}$ are the frequency and phase of the sinusoidal curve. The period of the oscillation is expected to be 90 ° [2], in accordance with the data shown in Fig. 7b. $E_{\mathrm{center,high}} - E_{\mathrm{center,low}}$ equals the ground-state splitting, and thus

$$E_{\mathrm{center,high}} - E_{\mathrm{center,low}} = g_{\mathrm{e}}^{\perp}\mu_{\mathrm{B}}B,$$

where $g_{\mathrm{e}}^{\perp}$ is the $g$-factor of the electron in the geometry used for measurements, $\mu_{\mathrm{B}}$ is the Bohr magneton, and $B$ denotes the applied magnetic field. With the values stated in Fig. 7b, we obtain a value of 1.91 for $g_{\mathrm{e}}^{\perp}$. $\Delta E_{\mathrm{excited,i}}$ (i = low, high) represents the splitting of the excited state, and thus can be used to calculate the hole $g$-factor $g_{\mathrm{h}}^{\perp}$ via

$$\Delta E_{\mathrm{excited,i}} = g_{\mathrm{h}}^{\perp}\mu_{\mathrm{B}}B.$$

From Fig. 7b, it can be seen that $\Delta E_{\text{excited,low}}$ is lower than $\Delta E_{\text{excited,high}}$, indicating that the high energy peak displays better polarization selectivity. Thus, $\Delta E_{\text{excited,high}}$ can be used to determine a value of 0.05 as a lower bound for $g_{\text{h}}^{\perp}$. These values obtained for the nanowire ensemble are consistent with the values obtained in the main text for a single dropcast nanowire.

## VI. OPTICAL PUMPING/REVERSE SPECTRAL HOLE BURNING

Fig. 8 shows photoluminescence spectra within the two electron satellite (TES) and longitudinal-optical (LO) phonon replica spectral region for a single nanowire under resonant excitation (In $D^0$-$D^0X$) with one or two lasers. The measurements were performed at 7 T ($\hat{c} \perp \vec{B}, \hat{k}$). The inset in Fig. 8 shows on which transitions the lasers are applied. Notably, the signal under two-laser excitation is larger than the sum of the signals obtained for single-laser excitation. This is the result of optical pumping. Under single-laser excitation, the system is spin-polarized, i.e., the population of electrons is transferred to the ground-state level where no laser field is applied. Therefore, in the steady-state, only a small fraction of electrons will remain in the ground-state level the single laser is applied to, and thus a small photoluminescence signal will be recorded. In contrast, under excitation with resonant lasers on two different ground state populations, electrons will be pumped back and forth between the ground state levels; therefore, neither ground-state will be fully depleted of electrons and an overall higher photoluminescence signal will be observed.

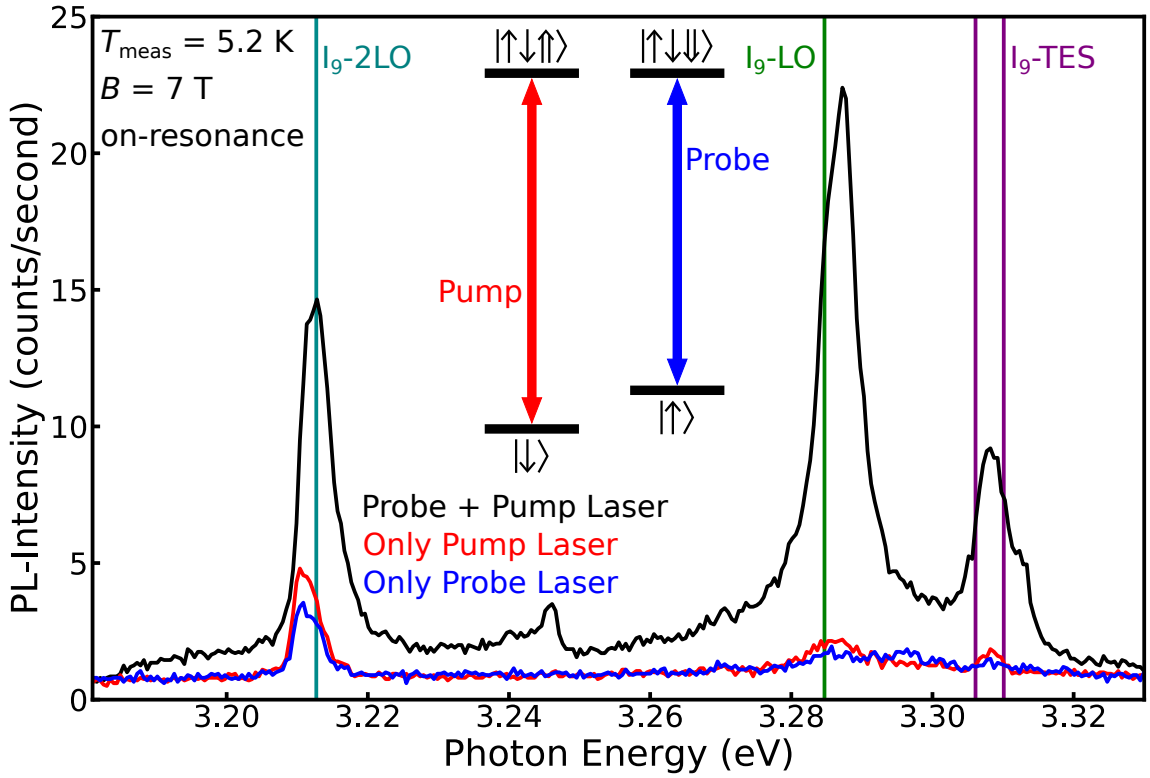



FIG. 8: Photoluminesence spectra of the two electron satellite (TES) and longitudinal-optical (LO) phonon replica spectral region for a single dropcast nanowire. It is the raw spectra used for the PLE in Fig. 2a of the main text. All measurements are at 7 T ($\hat{c} \perp \vec{B}, \hat{k}$) and 5.2 K. Both the pump and probe lasers have an excitation power of 7.2 µW. The inset shows an energy diagram illustrating the application of the laser fields. The probe laser is on-resonance with the In $|\uparrow\rangle \Leftrightarrow |\Downarrow \uparrow\downarrow\rangle$ transition. The pump laser is on-resonance with the In $|\downarrow\rangle \Leftrightarrow |\Uparrow \uparrow\downarrow\rangle$ transition. Individually, the pump and probe produce a small signal, because of optical pumping. With both pump and probe on at the same time the signal is greatly enhanced, because population is pumped back and forth between the $|\uparrow\rangle$ and the $|\downarrow\rangle$ states.

Fig. 9 displays PLE spectra under resonant single- and two-laser excitation for a nanowire ensemble for the In $D^0$-$D^0X$ transition. The measurements were performed at 7 T ($\hat{c} \parallel \vec{B}, \hat{k}$). The application of the laser fields is shown in the inset of Fig. 9. Under single-laser excitation, a low signal is observed due to optical pumping (see Fig. 8). Only a feature for the high-energy transition can be observed, indicating optical pumping is more efficient for the low-energy transition. The linewidth of the single-laser feature (∼30 GHz) is a combination of the effects of optical pumping and the ensemble linewidth. Under two-laser excitation, larger signals are observed due to the re-pumping of population between the two ground spin states. This recovered peak is also called a reverse spectral hole. The linewidths of the reverse spectral holes (10 - 20 GHz) are expected to reflect the linewidth of the In $D^0$-$D^0X$ transition that is the result of homogeneous broadening mechanisms and broadening mechanisms that are fast compared to our measurement time (∼20 s). Notably, the corresponding linewidths seen for single nanowires (see Fig. 10 and Fig. 2 (a) in the main text) are significantly wider, indicating an additional broadening mechanism affecting the linewidth of reverse spectral holes observed in single nanowires. Such mechanisms may be related to the higher excitation powers used for single nanowires.

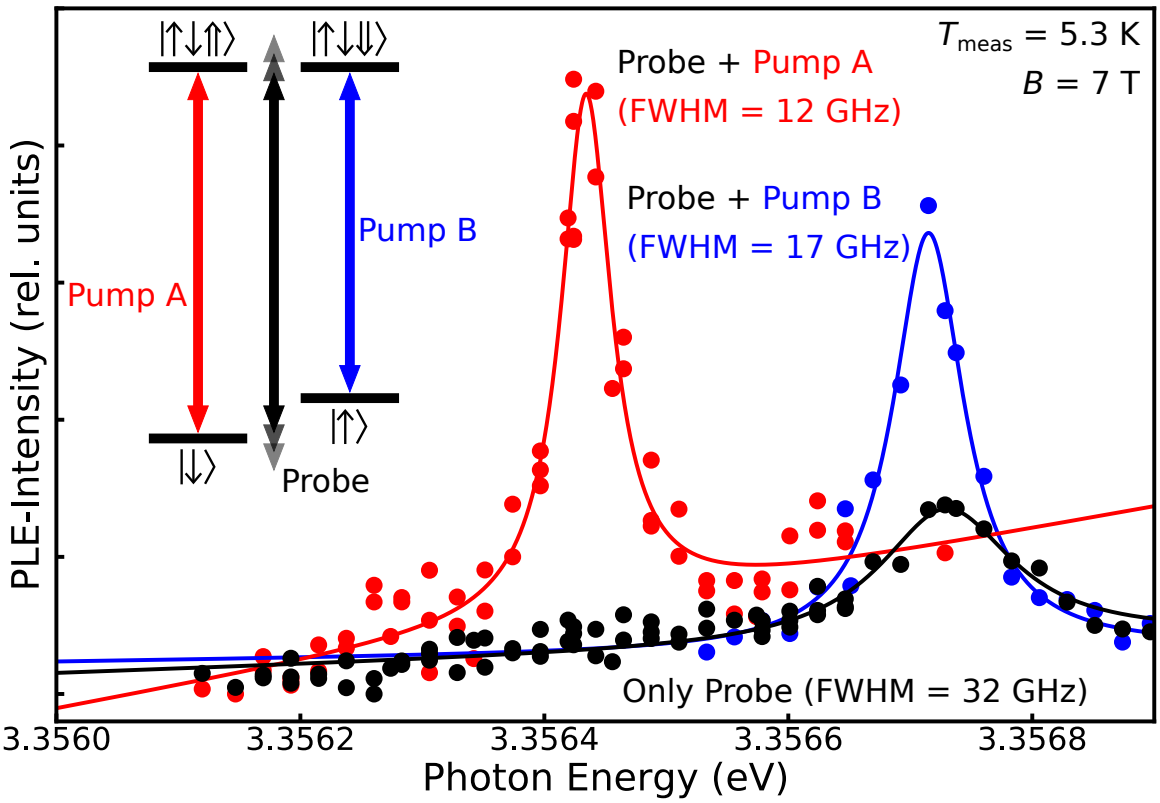



FIG. 9: In $D^0$-$D^0X$ PLE spectra of an ensemble of nanowires at 5.2 K and 7 T ($\hat{c} \parallel \vec{B}, \hat{k}$) with no pump (black), pump on the high energy transition (red), and pump on the low energy transition (blue). The inset shows an energy diagram illustrating the application of the laser fields. The excitation power is 200 nW for both pump and probe lasers. The solid lines are fits to the data. The two-laser datasets (red and blue) are offset for ease of comparison.

Fig. 10 displays PLE spectra under resonant single- and two-laser excitation for a single nanowire (nanowire #41) for the In $D^0$-$D^0X$ transition. The measurements were performed at 7 T ($\hat{c} \perp \vec{B}, \hat{k}$). The application of the laser fields is shown in the inset of Fig. 10. Under single-laser excitation, a low signal is observed due to optical pumping (see Fig. 8). Only a feature for the high-energy transition can be observed, indicating optical pumping is more efficient for the low-energy transition. The linewidth of the single-laser feature (∼60 GHz) is a combination of the effect of optical pumping and the ensemble linewidth. Under two-laser excitation, larger signals are observed due to the re-pumping of population between the two ground spin states. This recovered peak is also called the reverse spectral hole. The linewidth of the reverse spectral hole (∼50 GHz) is expected to reflect the linewidth of the In $D^0$-$D^0X$ transition that is the result of homogeneous broadening mechanisms and broadening mechanisms that are fast compared to our measurement time (∼20 s). However, significantly narrower linewidths are observed for the reverse spectral holes in the nanowire ensemble (see Fig. 9), indicating that there are additional mechanisms contributing to the width of the reverse spectral hole in the single nanowires. Such mechanisms may be related to the higher excitation powers used for single nanowires and would therefore include power broadening, spectral diffusion that is fast compared to our measurement time, and laser-induced temperature broadening.

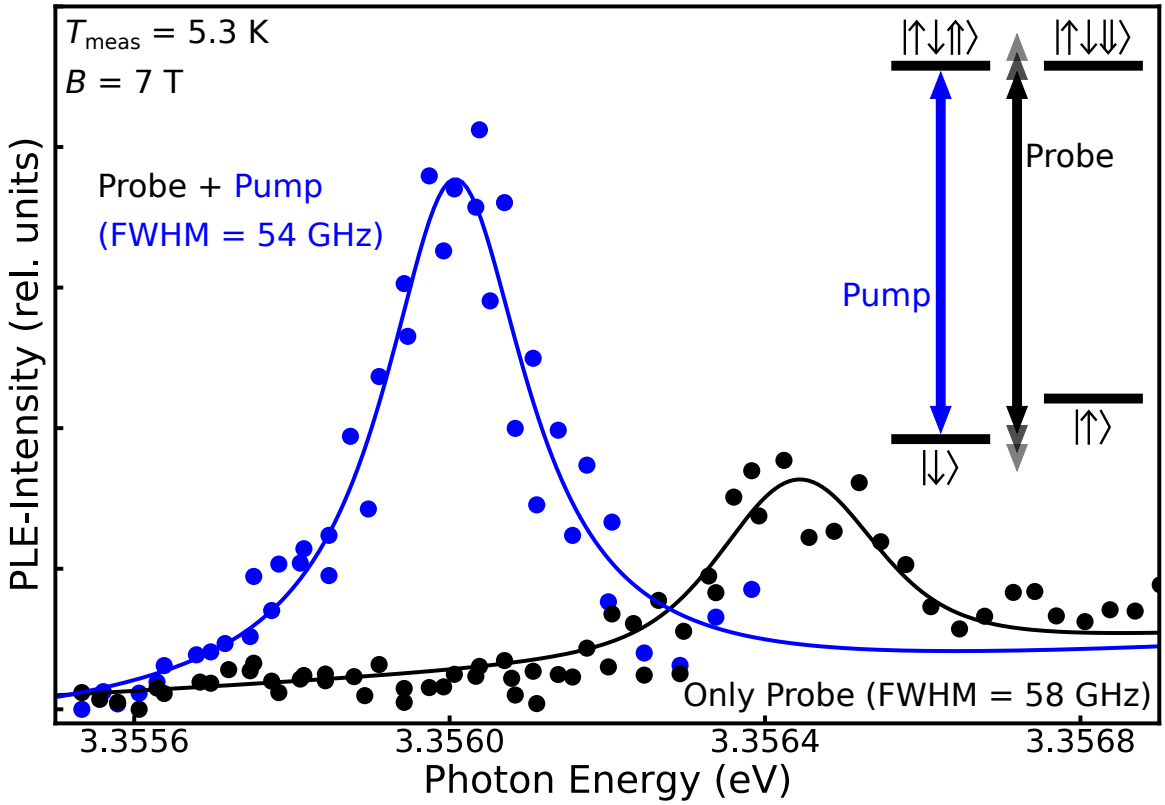



FIG. 10: In $D^0$-$D^0X$ PLE spectra of single dropcast nanowire #41. This is a different nanowire from the one shown in the main text. Measurements are performed at 5.2 K and 7 T ($\hat{c} \perp \vec{B}, \hat{k}$) with no pump (black) and the pump on the high energy transition (blue). The inset shows an energy diagram illustrating the application of the laser fields. The excitation power is 7.2 µW for both pump and probe lasers. The solid lines are fits to the data. The two-laser data (blue) is offset for ease of comparison.

Fig. 11 shows two-laser PLE for a single nanowire with different pump laser wavelengths near the In $D^0$-$D^0X$ transition. The measurements were performed at 7 T ($\hat{c} \perp \vec{B}, \hat{k}$). Fig. 11a is a PLE with the pump laser on-resonance with the In $|\downarrow\rangle \Leftrightarrow |\Uparrow\uparrow\downarrow\rangle$ transition. Fig. 11(b-g) are PLE with the pump laser shifted by the indicated energy. By comparing the shifted data (blue data) with the on-resonance data (black fit reproduced in each figure), we can see that as we go further off resonance the signal decreases and the linewidth increases. This further confirms that the two-laser recovered peak (reverse spectral hole peak) is related to the In $D^0X$ transition resonance and thus the re-pumping of population is between the two In $D^0X$ ground spin states.

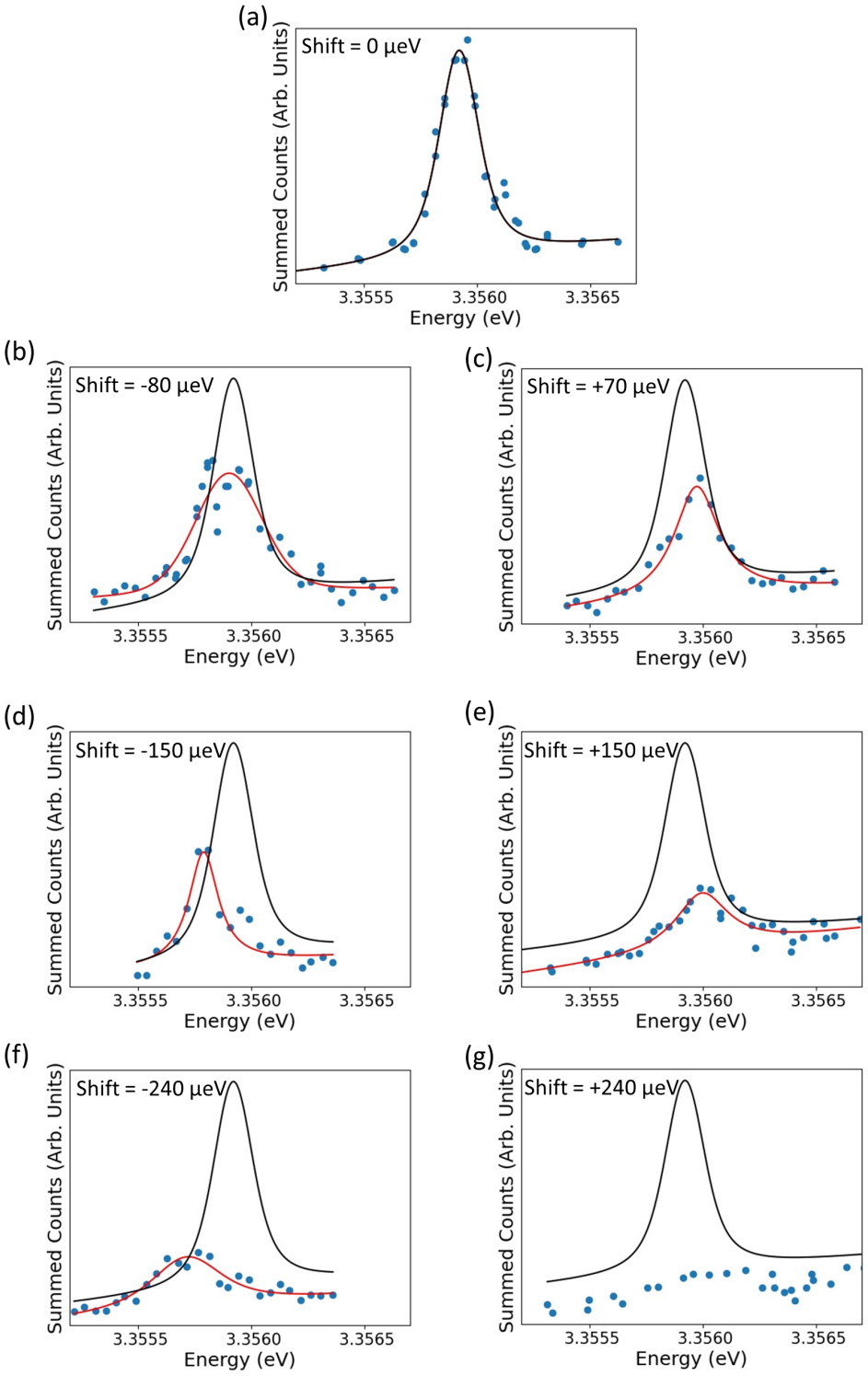



FIG. 11: Two-laser photoluminesence excitation (PLE) spectroscopy of a single dropcast nanowire. All measurements are performed at 7 T ($\hat{c} \perp \vec{B}, \hat{k}$) and 5.2 K. All laser powers are 7.2 μW. The probe laser is scanned over the In $|\uparrow\rangle \Leftrightarrow |\Downarrow\uparrow\downarrow\rangle$ transition while the two electron satellite (TES) and longitudinal-optical (LO) phonon replica luminescence is measured. (a) The pump laser is on-resonance with the In $|\downarrow\rangle \Leftrightarrow |\Uparrow\uparrow\downarrow\rangle$ transition. The black line is a fit to the data. (b-g) The pump laser is shifted from the resonance by the indicated amount. The red line is a fit to the data. The black line is the fit from (a) re-plotted to aid comparison. (g) The pump laser was detuned far enough that no re-pumping was allowed; therefore, the signal was below the noise floor.

## VII. COHERENT POPULATION TRAPPING

Fig. 12 shows a high-resolution PLE spectrum under two-laser resonant excitation for the In $D^0$-$D^0X$ transition. The measurements were performed at 7 T ($\hat{c} \perp \vec{B}, \hat{k}$). The application of the laser fields is shown in the inset of Fig. 12. Due to the effect of two-laser optical pumping a broad peak with a linewidth of ∼40 GHz can be seen (see Sec. VI and Fig. 10). A sharp dip with a linewidth of around 2 GHz can be seen in the center of the peak, indicating the occurrence of coherent population trapping. The measurements shown here were performed on a different single nanowire (nanowire #41) than the one shown in the main text.

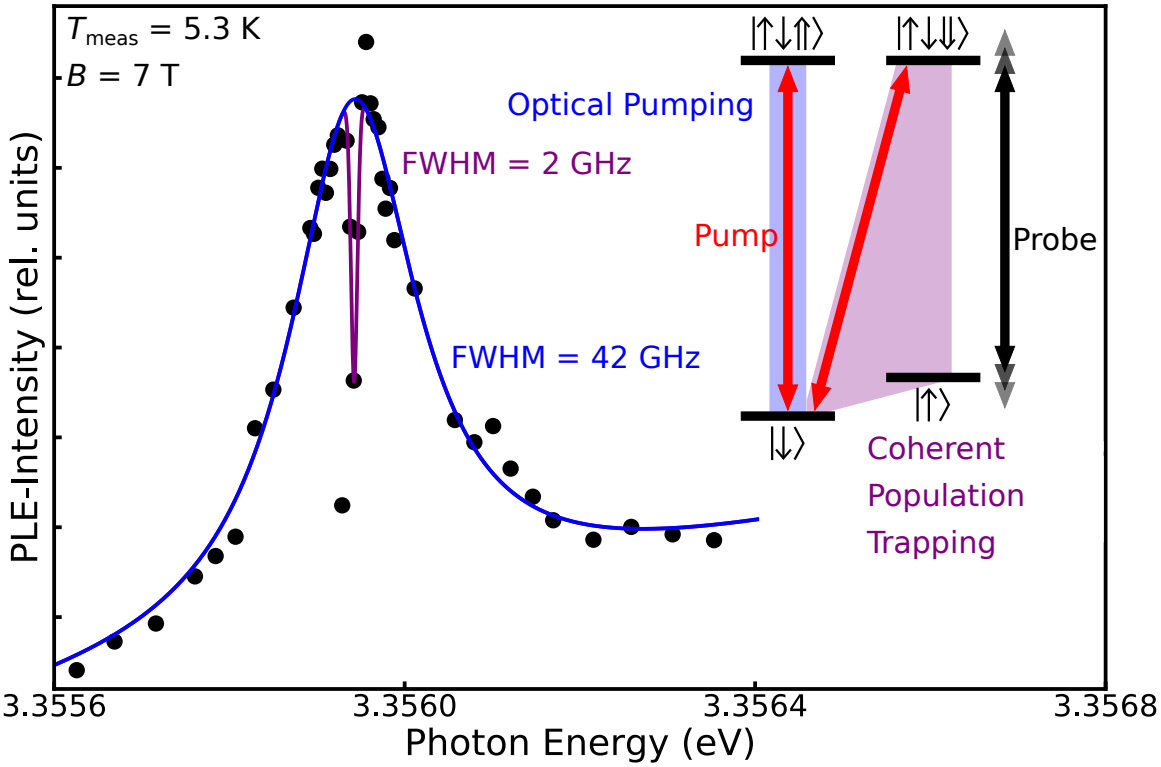



FIG. 12: High resolution, two-laser In $D^0$-$D^0X$ PLE spectrum of single drop-cast nanowire #41. This is a different nanowire from the one shown in the main text. The inset shows an energy diagram illustrating the application of the laser fields. Measurements are performed at 5.3 K and 7 T ($\hat{c} \perp \vec{B}, \hat{k}$). The excitation power is 7.2 µW for both pump and probe lasers. The solid lines are empirical fits to the two-laser optical pumping peak and the coherent population trapping dip.

The left panel of Fig. 13 shows PLE spectra recorded around the dip seen in Fig. 12 (nanowire #41). The measurements were performed at 7 T ($\hat{c} \perp \vec{B}, \hat{k}$). The application of the lasers fields is indicated in the inset of the right panel of Fig. 13. Measurements were performed at different powers for the pump lasers (7.2, 3.6, 0.4 µW). The right panel of Fig. 13 displays the linewidth of the CPT dip determined from an empirical Voigt fit. The linewidths observed on this single nanowire are similar to the CPT linewidths observed for the single nanowire discussed in the main text.

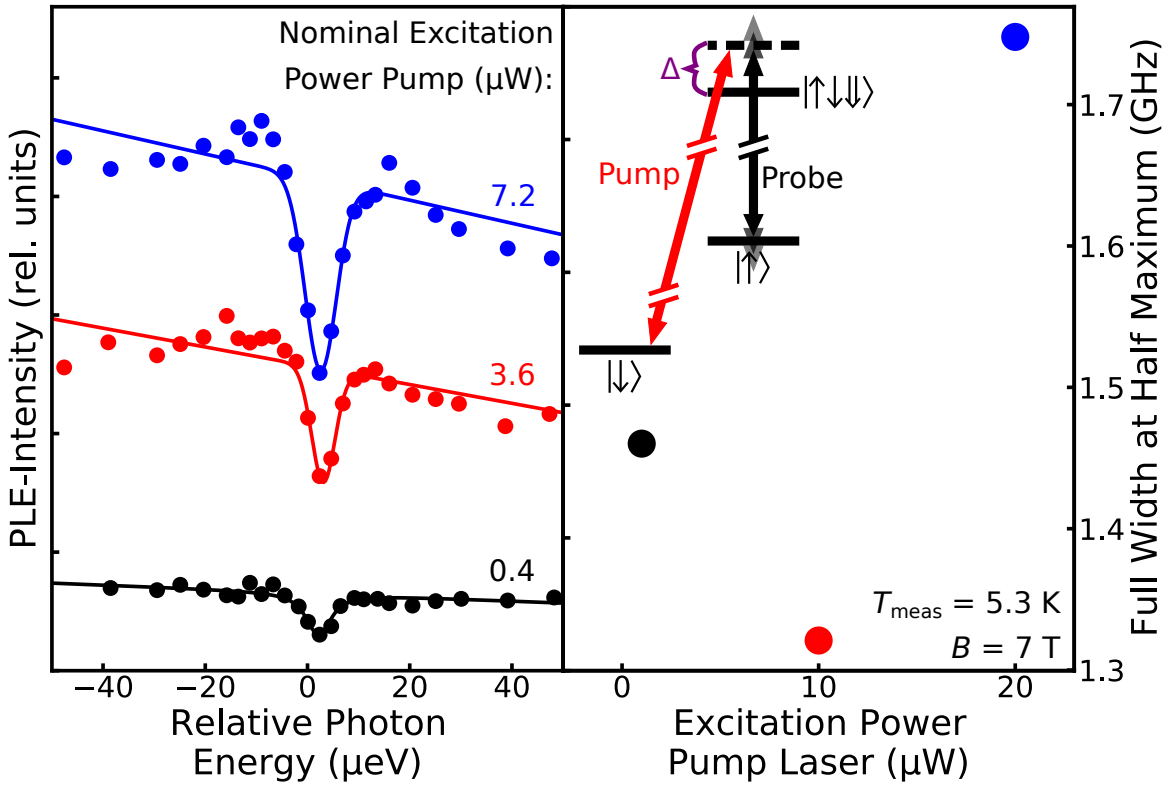



FIG. 13: Left panel: High resolution, two-laser In $D^0$-$D^0X$ PLE spectra of single dropcast nanowire #41 zoomed in on the coherent population trapping dip. This is a different nanowire from that shown in the main text. Measurements are performed at 5.3 K and 7 T ($\hat{c} \perp \vec{B}, \hat{k}$). The excitation power is 7.2 µW for the probe laser. The pump laser power is 7.2, 3.6, and 0.4 µW. The solid lines are empirical Voigt fits. Right panel: The fit full width half maximum as a function of pump power. The inset shows an energy diagram illustrating the application of the laser fields.

Fig. 14 shows PLE spectra recorded under two-laser excitation for the same single nanowire that is discussed in the main text. The measurements were performed at 7 T ($\hat{c} \perp \vec{B}, \hat{k}$). The probe laser was scanned across the same transition as indicated in the inset of Fig. 13. The pump laser was applied to the $|\downarrow\rangle \Leftrightarrow |\Uparrow\uparrow\downarrow\rangle$ transition but slightly shifted in energy in order to probe different two-laser resonance conditions, i.e., different values for $\Delta$. From the left panel of Fig. 14, it can be seen that the CPT dip as well as the peak of the reverse spectral hole shift when shifting the spectral position of the pump laser. The right panel of Fig. 14 quantitatively compares the shift of the CPT dip and the peak of the reverse spectral hole while changing the spectral position of the pump laser. Notably, the CPT shift is nearly one-to-one with the pump laser shift as expected from coherent population trapping. Indeed, the difference between the spectral position of the dip and the spectral position of the pump laser is 0.76-0.77 eV which is consistent with the expected ground-state splitting of 0.77 eV at 7 T assuming an electron $g$-factor of 1.90. This indicates that the electron and hole $g$-factors are close to what is expected from literature [2, 3] and what is seen in the nanowire ensemble sample in Sec. V. The shift of the peak of the reverse spectral hole does not occur one-to-one with the shift of the pump laser's spectral position; therefore, the reverse spectral hole's lineshape is not solely determined by the position of the pump laser, indicating spectral diffusion.

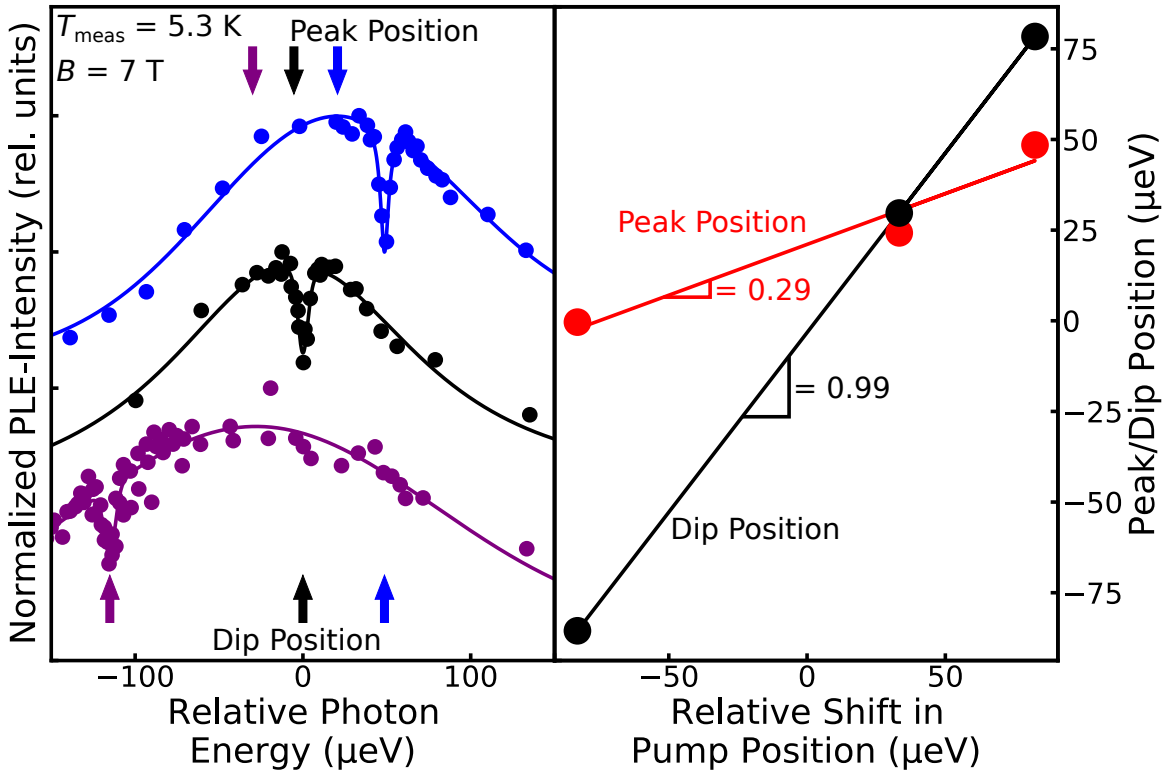



FIG. 14: High resolution, two-laser In $D^0$-$D^0X$ PLE spectra of the single drop-cast nanowire from the main text. The blue and black data is reproduced from the main text. All measurements are performed at 7 T ($\hat{c} \perp \vec{B}, \hat{k}$) and 5.3 K. All laser powers are 7.2 μW. The pump laser wavelength is shifted near the In $|\downarrow\rangle \Leftrightarrow |\Uparrow\uparrow\downarrow\rangle$ resonance. The left panel shows the PLE data with arrows indicating the fit peak and dip positions. The right panel shows the peak (red) and dip (black) positions as a function of the pump laser shift.

## VIII. SIMULATION OF LIGHT-GUIDING IN A NANOWIRE

In our single dropcast nanowire measurements, the excited state dephasing, and therefore our linewidths, are power broadened. However, we are unable to use less power in the current geometry because a minimal fraction of the light emitted by a nanowire lying horizontally on a substrate can be collected with an objective located above the nanowire.

To better understand how light is emitted from the nanowire, we visualize the electric field strength of a dropcast nanowire using finite difference time domain (FDTD) simulation. The defect emission is modeled as three dipole sources oriented in the x, y and z directions at the center of the nanowire. In the left panel of Fig. 15, The nanowire is simulated as lying on a substrate of 285 nm $SiO_2$ deposited on Si. The rectangle outlines the cross section (100 nm$\times$1 $\mu$m) of the nanowire and the horizontal lines divide materials with different indices of refraction. The electric field power has been guided to the ends of the nanowire and most of the energy flows into the substrate instead of the air due to the higher index of refraction.

To increase the collection efficiency, we envision isolating a single standing nanowire on a sapphire substrate and collecting light from the top of the nanowire to vastly enhance the efficiency of light extraction. Simulated in the right panel of Fig 15, the majority of the electric field power is guided to the ends of the standing nanowire; however, in this orientation the top end of the nanowire is far from the substrate and pointing toward the objective, allowing for a higher collection efficiency.

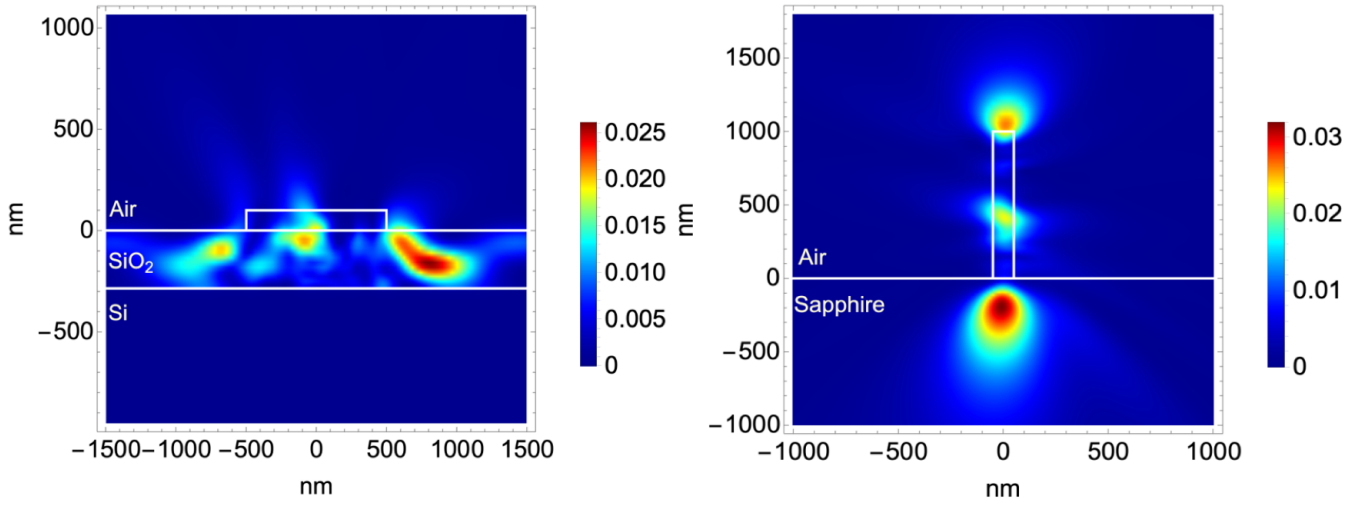



FIG. 15: Left: Electric field strength of a ZnO nanowire lying on a Si/$SiO_2$ substrate (285 nm $SiO_2$). Right: Electric field strength of a ZnO nanowire standing on a sapphire substrate.

[1] B. K. Meyer, H. Alves, D. M. Hofmann, W. Kriegseis, D. Forster, F. Bertram, J. Christen, A. Hoffmann, M. Straßburg, M. Dworzak, U. Haboeck, and A. V. Rodina, Physica Status Solidi (B) **241**, 231 (2004).
[2] M. R. Wagner, J. H. Schulze, R. Kirste, M. Cobet, A. Hoffmann, C. Rauch, A. V. Rodina, B. K. Meyer, U. Röder, and K. Thonke, Physical Review B **80**, 205203 (2009).
[3] L. Ding, B. K. Li, H. T. He, W. K. Ge, J. N. Wang, J. Q. Ning, X. M. Dai, C. C. Ling, and S. J. Xu, Journal of Applied Physics **105**, 053511 (2009).